Saudi Journal of Biological Sciences 27 (2020) 2993–3002

Contents lists available at ScienceDirect

Saudi Journal of Biological Sciences

journal homepage: www.sciencedirect.com

Original article

Ganoderma lucidum inspired silver nanoparticles and its biomedical applications with special reference to drug resistant *Escherichia coli* isolates from CAUTI

Mysoon M. Al-Ansari [a,*], P. Dhasarathan [b], A.J.A. Ranjitsingh [b,*], Latifah A. Al-Humaid [a]

[a] Department of Botany and Microbiology, Female Campus, College of Science, King Saud University, Riyadh, Saudi Arabia
[b] Department of Biotechnology, Prathyusha Engineering College, Chennai 600056, India

ARTICLE INFO

Article history:
Received 24 July 2020
Revised 31 August 2020
Accepted 2 September 2020
Available online 10 September 2020

Keywords:
Ganoderma lucidum
Urinary tract infection
Antibacterial activity
Antioxidant
Breast cancer cell line

ABSTRACT

In the search for alternative therapy for infections and other ailments, metallic nanoparticles, mainly silver nanoparticles (AgNPs) synthesized through bioengineered sources are extensively explored. Fungal bioactive compounds and their nanoparticles were reported with the potential biomedical application. A medicinal mushroom *Ganoderma lucidum* was reported as a repository of rich medicinal properties. In the current study, silver nanoparticles were synthesized using the extracts of *G. lucidum* and its antimicrobial activity was tested against drug-resistant *Escherichia coli* isolated from the catheter used for urinary tract infection (CAUTI). The GC–MS study of *G. lucidum* extracts showed the presence of ethyl acetoacetate ethylene acetal with the highest area percentage of 72.2% and retention time (RT 5873). Pyridine-3-ol is the second primary compound with a peak height of 6.44% and a retention time of 2.143. The third compound is l,4-Dioxane-2,3-diol, with an area of 8.09% and RT 5450. Butylated Hydroxy Toluene [BHT] is the fourth major compound with an area of 3.32%, and 9-Cedranone constitutes the fifth position in occupying the area percentage [1.88] and height 1.56%. Pyrrole is the sixth primary compound registering an area size of 0.96% and height 2.06%. The AgNPs synthesized using *G. lucidum* extract were in size range 23 and 58 nm as per SEM analysis and within the range wavelength 0.556–0.796 nm as per UV–Vis spectral study. FTIR Spectroscopy and X-ray diffraction analysis (XRD) were made to characterize the formed nanoparticles. The AgNPs synthesized effectively inhibited the growth of *E. coli* isolated from catheter-associated urinary tract infection and showed resistance to many drugs. The antioxidant potential of the synthesized nanoparticles assessed using DPPH radical scavenging activity, EC50 (μg/ml), and ARP data showed that the prepared nanoparticles were more potent in free radical scavenging activity than the standard quercetin. The cytotoxicity effect of Ag-NPs on breast cancer cell line- MDA-MB-231 confirmed its anticancer potential. The half-maximal inhibitory concentration (IC_{50}) of Ag-NPs to inhibit 50% of the tumor was 9.2 g/mL. The synthesized GL-AgNPs was exhibited a multifocal biomedical potential.

1. Introduction

A catheter is a medical device primarily used for draining the urine after surgeries and for the patients who suffer from urine incontinence. Prolonged implantation of the catheter enables the pathogenic microbes to form a biofilm around it. Biofilm-associated bacteria leads to severe infections (Sandhu et al., 2018). The catheter-associated urinary tract infections (CAUTI) lead to risk factors if the duration of catheterization is extended. It paves the way for developing bacteriuria (Kim et al., 2017). The long term indwelling of catheters promotes polymicrobial infection from bacteria and yeast and subject to a broad treatment spectrum (Inga et al., 2007). Worldwide, millions of people using

* Corresponding authors.
E-mail addresses: soona70@yahoo.com (M.M. Al-Ansari), ranjitspkc@gmail.com (A.J.A. Ranjitsingh).

Peer review under responsibility of King Saud University.

Production and hosting by Elsevier

https://doi.org/10.1016/j.sjbs.2020.09.008
1319-562X/

catheters have become victims of CAUTI, ending in morbidity and mortality and severe damage to health systems (Harding and Reynolds, 2014; Muramatsu et al., 2018). Medical complications like catheter encrustation, bladder stones formation, septicemia, cystitis desiccation of urinary bladder, endotoxic shock, and pyelonephritis are associated with CAUTI (Sabih and Leslie, 2020). The common symptoms of CAUTI include cloudy urine, odor in the urine, fever, vomiting, blood in the urine, unexplained fatigue, and chills, endotoxic shock, cystitis and several other medical complications such as the mechanical trauma and mobility impairment. The CAUTI is reported to cause endotoxic shock, cystitis, and several other medical complications such as mechanical trauma and mobility impairment (Bhani et al., 2017). The pathogenic microbial cover over the indwelling urethral catheter and the interactions among the pathogens associated with the biofilm formation on the catheter makes the microbes to resist many antibiotic drugs (Sandhu et al., 2018). The presence of a catheter for a longer period, normally over seven days, inflicts bacteriuria even after one month (NICE, 2009). Bacterial biofilms are reported to be highly recalcitrant to antibiotic therapies because of multiple tolerance mechanisms (Olivares et al., 2020; Kamali et al., 2020; Hrvatin, 2017). Kaul et al. (2019) recommended alternative therapies for antibiotics to Combat Drug-Resistant Bacterial Pathogens. Among the different alternative treatments, the silver nanoparticles were suggested very effective therapeutic methods according to earlier reports (Muramatsu et al., 2018).

Because of increasing microbial multidrug resistance, there is a need for novel therapeutic approaches to replace ineffective antibiotics. Attention is focused on Nano-scale antimicrobial therapies. This search confirmed that silver nanoparticles have unique antimicrobial properties (Inamuddin, 2020). The biosynthesis of silver nanoparticles using the eco-friendly biological agents, plants, or microbial agents that function as reducing and capping agents further replaces the chemically synthesized nanoparticles (Roy et al., 2019).

Hence in the present study, biosynthesis of silver nanoparticles was synthesized using medicinal mushroom *G. lucidum* extract, and it is planned to test its antimicrobial action against CAUTI isolates. *G. lucidum* is a Basidiomycetes fungus belonging to the family of Polyporaceae. *G. lucidum* has antimicrobial effect due to bacteriolytic enzyme presence, lysozyme and acid protease had used *G. lucidum* for the prevention and the treatment of the various diseases (Inamuddin, 2020). Since ancient times *G. lucidum* is reported as a super immune stimulant that strongly protects the entire body (Cor et al., 2018). It has antitumor, immune-modulatory, cardiovascular, respiratory, anti-hepatotoxic, and anti-nociceptive (active against pain) effect. *G. lucidum* ehhibits anti-atherosclerotic, anti-inflammatory, anti-diabetic, anti-oxidative, anti-aging, antifungal, antiviral and immunity-boosting action (Zhang et al., 2014; Cilerdzic et al., 2018; Liu et al., 2016; Nanhui et al., 2020). Aranzazu et al. (2020) in their review on *Ganoderma lucidun* reported it as an edible mushroom since 2700 BCE. The biomedical applications of metal-based nanoparticles promote non-specific bacterial toxicity mechanisms (Sánchez-López et al., 2020). Earlier workers also reported the antibacterial activity of AgNPs (Kannan et al., 2014; Ranjith et al., 2017; Alfuraydi et al., 2019; Devanesan et al., 2020; AlSalhi et al., 2016). In the present research, silver nanoparticles were prepared using the ethanol extracts of *G. lucidum*, and its biomedical applications were traced.

2. Materials and methods

2.1. Collection and extraction of Ganoderma lucidum

The *Ganoderma lucidum* is an edible mushroom and their dried fruiting bodies are available in the commercial market. The dried mycelia and the fruiting bodies of *G. lucidum* were obtained from Beshan Trading private limited, Chennai. The phytochemical constituents of *G. lucidum* mycelia were extracted using ethanol through hot extraction methods. Briefly, twenty gram of *G. lucidum* powder was dissolved in 200 ml of 70% ethanol and kept the Soxhlet apparatus for the hot extraction process. The extract was then stored in a refrigerated condition for further use.

2.2. Phytochemical constituents analysis by GC–MS

The phytochemical constituents of the *G. lucidum* extraction were obtained with GCMS analysis. Briefly, *G. lucidum* extraction was subjected to GC–MS, (Shimdzu GC-2010 Plus gas chromatograph). It was equipped with a straight deactivated 2 mm direct injector liner and a 15 m Alltech EC-5 column (250 μ I.D., 0.25 μ film thickness). A split injection was used for sample introduction, and the split ratio was set to 10:1. The oven temperature program was programmed to start at 35 °C, hold for 2 min, then ramp at 20 °C per minute to 450 °C and hold for 5 min. The helium carrier gas was set to 2 ml/minute flow rate (constant flow mode). A metal quadrupole mass spectrometer equipped with a highly sensitive and stable ion source operating in electron ionization (EI) mode with software GCMS solution ver. 2.6 was used for all analyses. Mass spectra with low-resolution were obtained at a resolving power of 1000 (20% height definition) and scanning from m/z 25 to m/z 1000 at 0.3 s per scan with a 0.2-second inter-scan delay.

2.3. Synthesis of G. lucidum extracts AgNPs (GL-AgNPs)

The AgNPs were synthesized according to the method described by Devanesan et al. (2020). In brief, 9 ml of 1 mM of $AgNO_3$ (0.042 g in 100 ml of distilled water) was taken in a sterile conical flask. It was kept on the hot plate, followed by magnetic stirring, and the temperature was set at 70 °C. After 1 ml of ethanol extract of *G. lucidum* was added to the 1 mM silver nitrate solution. The nanoparticle formation was determined by continuous stirring and heating solution, and finally, the reddish-brown colour change was observed. The same procedure was carried out for the remaining four different volumes of *G. lucidum* extracts and silver nitrate solution.

Further, the solution was kept in an ultrasonic bath for 30 min, and it was subjected to 360 W microwave irradiation for 5 min. The mixture was centrifuged for 30 min at 10000 rpm at 4 °C. The supernatant was discarded, and colloidal silver was washed several times with deionized water to remove contaminations. Finally, Ag-NPs were dried at 60 °C in a hot air oven, and the nanoparticles pellets were powdered, lyophilized, and kept at room temperature for further work.

2.4. Characterization of GL-AgNPs

2.4.1. UV–Vis spectroscopy study

The optical density (OD) values of the synthesized silver nanoparticles with different volumes of *G. lucidum* extract and $AgNO_3$ solution were observed with the help of UV–Vis spectroscopy, Perkin Elmer (USA) scanning ranges at 200–800 nm. The UV–Visible spectral studies confirmed the nanoparticle formation.

2.4.2. X-ray Diffraction Analysis (XRD)

For XRD study, the powdered AgNPs were used. The diffraction pattern was recorded in an angle range of 20–80° at a 2θ pattern. For XRD study, the powdered AgNPs were used. The diffraction pattern was recorded with Kα radiation (λ = 1.54059 nm) in an angle range of 20–80° at a 2θ pattern [X-ray diffractometer Ultima

IV, Rigaku, Japan). The resultant image was compared with the standard JCPDS data.

2.4.3. Scanning Electron Microscopy (SEM)

The surface morphology and structure of the nanoparticles were further studied using SEM. The morphological characters of synthesized nanoparticles were done up to 100 nm, and the images were recorded using JEOL SM-7600F, (Japan).

2.4.4. FTIR spectroscopy

FTIR-ATR was also used to ascertain the structure of particles. FTIR-ATR study in the range of 250–5000 cm^{-1} was noted for each spectrum at a resolution of 4 cm^{-1} (Shimadzu 8400S spectrophotometer with OPUS 6.0 software, Billerica, MA, USA)

2.5. Escherichia coli isolation

For the antimicrobial evaluation of synthesized silver nanoparticles, drug-resistant *Escherichia coli* strains isolated from CAUTI patients were used. Although many bacteria showed drug resistance, *E. coli* is a severe drug-resistant nosocomial pathogen. In the preliminary screening, The isolate that showed resistance to more than 12 antibiotics was isolated for further identification using standard biochemical and physiological characterization methods described by Bergey and Holt (2000) and specific medium. To isolate bacteria associated with urinary tract infection patients who have given urine sample to Vivek Pathology laboratory Tamilnadu, India was used after getting the patients' written consent. The midstream urine sample of 5 females with uncomplicated UTIs was collected and immediately cultured after collection. About 5 ml of urine was aspirated into a sterile syringe and transferred in a sterile urine collector bottle for further study. Then 1 ml of each urine sample collected from each patient was taken in separate sterile centrifuge tubes. Then the tubes were centrifuged at 5000 rpm for about 20 min. The pellets were collected and cultured on MacConkey's agar and nutrient agar plates. After the biochemical and strain-specific medium tests, computer-based identification was made by using the API 20E system (bioMérieux SA, Marcy l'Etoile, France). The identified, *E. coli* strain was named and stored in the PEC Biotech lab bacterial collection (Pec /Ut/E.col/11/20)

2.6. The antimicrobial bacterial activity of GL-AgNPs

2.6.1. Microbial pathogen

For the antimicrobial evaluation of synthesized silver nanoparticles, drug-resistant *E. coli* strains isolated from catheter-associated urinary tract infection (CAUTI) patients were used. The four drug-resistant isolates E1, E2, E3 and E4 were performed for antimicrobial sensitivity study with synthesized GL-AgNPs.

2.6.2. Antibiotic sensitivity assay

The antimicrobial activity of GL-AgNPs was evaluated by the well diffusion method. Muller Hinton agar (MHA) medium was prepared, and after autoclaving, it was cooled and poured into plates. A loop full ($5x10^5$ CFU/mL, McFarland standard) of *E. coli* culture isolates were swabbed onto MHA plates with a sterile cotton swab. Then 6 mm diameter well was made in the agar plates using a sterile cork borer. With the sterile micro pipette's help, the wells were filled with different concentrations *viz*., 25, 50, and 75 mg/mL of GL-AgNPs. The ciprofloxacin (5 mcg) and Dimethyl sulfoxide (DMSO) were positive and negative control, respectively. After that, the plates were incubated at 37 °C for 24 h in an incubator. After incubation, the zone of inhibition was observed, and the diameter was measured in mm. Each treatment was performed in triplicate. The mean and standard error was calculated using the measurements taken from the triplicates.

2.7. An antioxidant study using DPPH (1,1-diphenyl–2–picrylhydrazyl) radical scavenging assay

The antioxidant potential of biosynthesized GL–Ag NPs was tested by DPPH method. DPPH free radical scavenging activity was carried out in a 96-well microplate described by Boly et al. (2016). From the stock solution of synthesized GL-AgNPs dissolved in DMSO, different concentrations (5, 10, 15, 20, and 25 μg/mL) were prepared and mixed with 100 μL of 0.01% methanolic solution containing DPPH radicals. After vortexing, the reaction mixture was left undisturbed in a dark room for 30 min. Then the absorbance was recorded at 517 nm using a UV–Vis spectrophotometer. The standard used was quercetin, and it was also prepared at different concentrations (5, 10, 15, 20, & 25 μg/mL). The DPPH radical scavenging activity was calculated as: DPPH scavenging activity (%) = [(Abs control − Abs sample)/(Abs control)] × 100. Abs = absorbance of the control and Abs = absorbance of extract. The results were expressed as which is The concentration of the sample required to inhibit 50% of DPPH concentration (IC50) was taken as the inhibition activity.

2.8. Cell culture and cytotoxicity assay

For a cytotoxic study on tumor cells, MTT assay was used (Gurunathan et al., 2013). The MDA-MB-231 human breast cancer cells (ATCC HTB-26) were used to evaluate anti-tumor potential of synthesized AgNPs. The cell line was maintained in Dulbecco's modified Eagle's medium (DMEM) with 10% fetal bovine serum (FBS) supplementation and 1% penicillin antibiotic solution. Cells were grown to the confluence at 37 °C and 5% CO_2 atmosphere. After that, a single-cell suspension was prepared using 2% trypsin-EDTA. After this trypsin addition, the cell suspension was adjusted to 1×10^6/ml. Then 100 μL (10^6 cells) of new cell suspensions were seeded into each well of 96-well plate containing different concentrations of GL-AgNPs (5, 10, 15, 25 and 100 μg/mL). The culture plate was incubated for 24 h at 37 °C in a humidified incubator. Briefly, 10 μL of MTT (5 mg/mL in PBS) was added to each well, after 24 h of incubation (37 °C, 5% CO_2 in a humid atmosphere). The plate was again incubated for 4 h at 37 °C. The formazan formed after that period was carefully dissolved in 100 μL of DMSO with gentle shaking at 37 °C. With the help of an ELISA reader (Spectra MAX; Molecular Devices, USA) the absorbance was measured at 595 nm. The mean of three independent measurements was taken, and the concentrations of GL-AgNPs showing a 50% reduction in cell viability (i.e., IC50 values) were then calculated.

3. Results and discussion

3.1. GCMS analysis

The collection and extraction of bioactive components from *G. lucidum* are given in Fig. 1(a and b). The phytochemical constituents in the *G. lucidum* mycelia were extracted using ethanol as solvent through the Soxhlet apparatus. Twenty grams of *G. lucidum* powder was dissolved in 200 ml of 70% ethanol and kept at room temperature for about seven h. The extract was then stored in a refrigerated condition for further use. The phytochemical constituents present in *G. lucidum* extraction were identified with GCMS analysis. The compound present is ethyl acetoacetate ethylene acetal (RT 5873), which has the highest area percentage of 72.2%. The second major compound Pyridine-3-ol showed a peak

Fig. 1. (a) *G. lucidium* (Basidiomycota Fungi); (b) Ethanolic extract of *G. lucidum using* Soxhlet apparatus.

height of 6.44% and a retention time of 2.143. The third compound is l, 4-Dioxane-2,3-diol (RT 5450). It showed an area percentage of 8.09% and a height percentage of 5.83%. Butylated Hydroxy Toluene [BHT] (RT 19.725) is the fourth compound occupying an area of 3.32% and height percentage of 3.61%, followed by this 9-Cedranone constitutes the fifth position in occupying the area percentage [1.88] and height 1.56percent, Pyrrole is the sixth compound registering an area size of 0.96% and height2.06%. The other twenty-one compounds are in a lesser amount. From the chemical structure, it is inferred volatile compounds are maximum in the ethanolic extract of *G. lucidum* (Fig. 2 and Table 1). The GC–MS chromatogram of ethanolic extract of the mycelium of *G. lucidum* showed six (6) bioactive compounds (Fig. 1) with a good peak mood. The interpretation of the mass spectrum identified 27 compounds of ethanol extract of *G. lucidum*. Table 1 shows the compounds' name, peak area %, retention time (RT), and nature of compound; many of the bioactive compounds screened in the ethanolic extract are having medicinal value and volatile.

In *G. lucidum* triterpenoids and polysaccharides were the prime pharmacologically active compounds executing medicinal properties including antimicrobial, anticancer activities, and antiviral action against influenza a virus, human immunodeficiency virus and dengue virus (Bharadwaj et al., 2019). So the extracts of *G. lucidum* with high therapeutic potential are likely to synthesize silver nanoparticles with a high action potential. It is reported that the mycosynthesis of silver nanoparticles using fungi enhances a wide range of applications of nanoparticles, including health and agriculture. The capping developed in the nanoparticles due to the action of phytoconstituents derived from the fungi, confer stability to the nanoparticles, and help in the formation of protein capping that help in the anchoring of drugs and genetic material transport into cells (Zhang et al., 2016). The capping also reported exhibiting biological activity, synergistic with the nanoparticle core. In the present study, the ethanolic extract of *G. lucidum* screened through CC-MS reported 27 bioactive compounds. It is also said that G. *lucidum* contains more than 400 bio-active compounds like polysaccharides, triterpenoids, proteins, enzymes, steroids, sterols, nucleotides, fatty acids, vitamins, and minerals. In the biosynthesis of NPs, electron exchange from a donor molecule leads to precipitation ion of as nanoparticle, which is facilitated by the enzymatic system. The other secondary metabolites also influence electron exchanging (Moghaddam et al., 2015). As *G. lucidum* is reported to have such biomolecules, their role in reducing silver into silver nanoparticles and equipping the nanoparticle with caps and therapeutic potential is realistic to promote the *G. lucidum* engineered silver nanoparticles with multifold action. Also, enzymes like α-NADPH-dependent nitrate reductase, phytochelatin, and glutathione reductase FAD-dependent can reduce ions of the toxic metal to become nanoparticles (Scott et al., 2008). In *G. lucidum*, the synthesis of GLCPR, an NADPH-CYP reductase, was reported.

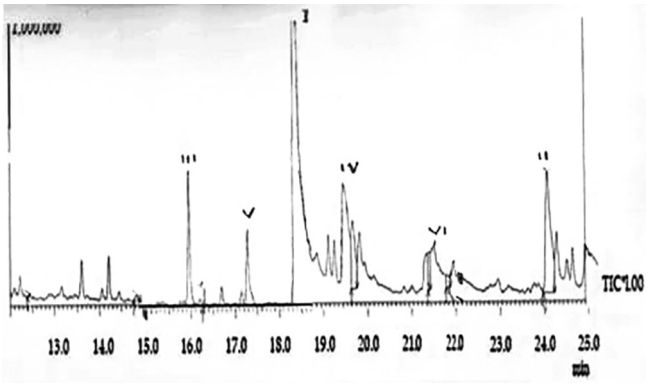

Fig. 2. Chromatogram showing the photochemical constituents of *G. lucidium* extracts: I. Ethyl acetoacetate ethylene acetal; II. Pyridine-3-ol; III. l4-Dioxane-2,3-diol; IV. Butylated Hydroxy Toluene; V. 9-Cedranone & VI. Pyrrole.

3.2. Optimization of prepared nanoparticles

The *G. lucidum* hot extract was a pale green color, and after the formation of nanoparticles, the color of the solution turned reddish-brown as an indication of AgNPs (Fig. 3). As the particles get into a smaller size, the surface plasmon resonance gets tuned, and a color change develops in the nanoparticle solution. The optical density (OD) values of the synthesized silver nanoparticles with different volumes of *G. lucidum* extract and AgNO3 solution were observed with the help of UV spectroscopy between 0.394 and 0.545 nm. The test tube 4, which consists of 4 ml of *G. lucidum* extract and 6 ml of AgNO3 solution with the absorbance of 0.456 nm, was used further to analyze antibacterial activity of silver nanoparticle against *E. coli* since its absorbance was within the optimum range (0.450–0.460 nm).

3.3. UV–Vis spectroscopy

The optical density (OD) values of the synthesized silver nanoparticles with different volumes of *G. lucidum* extract and $AgNO_3$ solution were observed with the help of UV–Vis spectroscopy between 0.394 and 0.545 nm (Fig. 4). The surface plasmon band centered at ~450 nm indicated the presence of silver nanoparticles. The UV–vis spectrum is a fundamental but effective

Table 1
Phytochemical constituents of *G. lucidium* extracts.

Peak	R. Time	Name	Area	Area%	Height	Height%
1	5.450	l,4-Dioxane-2,3-diol	3,059,358	8.09	353,252	5.83
2	5.837	Ethyl acetoacetate ethylene acetal	27,275,950	72.12	4,463,568	73.64
3	6.200	Glyodin	6797	0.02	5380	0.09
4	6.737	p-Menthon-8-thiol	72,418	0.19	15,516	0.26
5	6.842	n-Valeric acid *cis*-3-hexenyl ester	14,014	0.04	4862	0.08
6	7.150	D-Serine	48,969	0.13	18,451	0.30
7	7.350	Piperidine	104,081	0.28	22,099	0.36
8	7.417	Ketone, isopropylidenecyclo propyl methyl	35,281	0.09	9707	0.16
9	8.099	9-Cedranone	711,546	1.88	94,350	1.56
10	8.789	5,6-bis(2,2-dimethylpropylidene)-	23,617	0.06	11,138	0.18
11	10.200	n-Propyl nonyl ether	163,668	0.43	49,326	0.81
12	10.382	4-Methoxyphenylethylamine,	490,142	1.30	66,372	1.10
13	10.692	3-(phenylmethyl)-3-Benzylpyridine	109,444	0.29	25,933	0.43
14	11.858	Ethylene diacrylate	87,239	0.23	26,023	0.43
15	12.419	Decyl .alpha.-d-glucoside	14,010	0.04	9667	0.16
16	14.835	.alpha.-D-Mannopyranoside	78,687	0.21	21,306	0.35
17	16.275	4-Aminocyclohexanol acetate	8368	0.02	6597	0.11
18	19.725	BHT	1,257,208	3.32	218,545	3.61
19	21.467	Pyrrole	363,728	0.96	123,924	2.04
20	21.908	Adamantane-1-carboxamide, N-(4- chlorobem	189,281	0.50	35,536	0.59
21	24.153	Pyridin-3-ol	3,209,303	8.49	390,278	6.44
22	28.708	Methyl octyl ether	49,748	0.13	22,526	0.37
23	31.957	Succinic acid,	301,269	0.80	39,468	0.65
24	35.375	Diethylene glycol dibenzoate	18,765	0.05	8685	0.14
25	40.450	Piperazine	13,597	0.04	6121	0.10
26	40.600	Ethyl acetopyruvate	35,090	0.09	4722	0.08
27	41.406	.alpha.-D-Xylopyranoside	81,039	0.21	7975	0.13

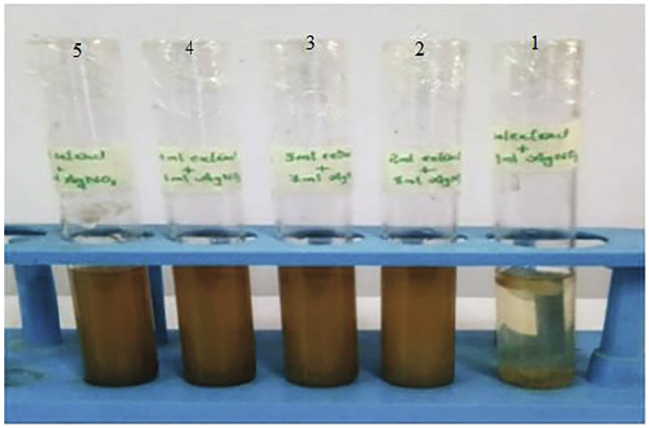

Fig. 3. Optical photographs of Ganoderma extract and silver nitrate mixture in different proportions and Color changes indicating formation of AgNPs (1. 1:9 – pale green colour -pre NPs formation; 2. 2:8 – Progressing dark brown; 3. 3:7 – Progressing dark brown; 4. 4:6 – Reddish brown showing AgNPs formation; 5. 5:5 – Reddish brown showing AgNPs formation).

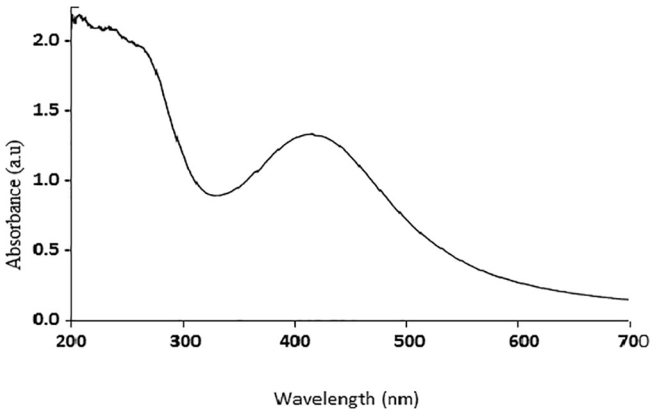

Fig 4. UV–Vis spectrum of synthesized GL-AgNPs.

technique to confirm the formation of metal nanoparticles having surface plasmon resonance (SPR). The absorption peak at 450 nm at different time intervals (Fig. 4) conforms the plasmon resonance recorded for silver nanoparticles (AlSalhi et al., 2016; Alfuraydi et al., 2019). The synthesized GL-AgNPs characterized with an absorption peak at 450 nm indicates the constancy of synthesized GL-AgNPs. It was suggested that an SPR peak present between 410 and 450 nm confirms the AgNPs formation and its spherical nature of nanoparticles (Zaheer and Rafiuddin, 2012).

3.4. Fourier Transformed Infrared Spectroscopy

The FT-IR spectrum of *G. lucidum* extract is given in Fig. 5. The FTIR spectral values show five peaks at 1480, 1510, 1560, 1590, and 1680 cm^{-1} wavelength. The absorption wavelength between 1590 and 1680 cm^{-1} indicates a good C=C stretching vibration

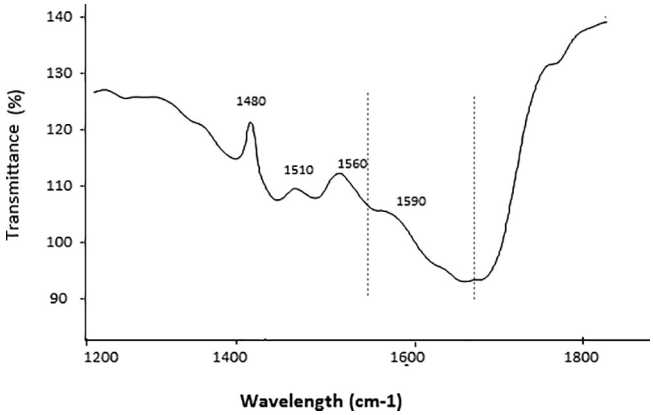

Fig. 5. FTIR spectrum of synthesized GL-AgNPs.

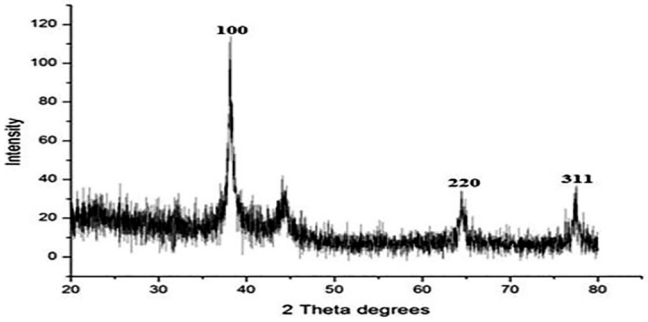

Fig. 6. XRD spectrum of synthesized GL-AgNPs.

due to diatomic units' vibrations. It is an excellent aromatic ring stretch also. The infrared wavelength between 1550 and 1500 cm^{-1} means a strong N—O stretching due to nitro compound. The absorption wavelength between 1610 and 1420 indicates carbonyl compound -Carboxylate (carboxylic acid salt). The stretch between 1680 and 1630 means the Amide compound, and the wavelength between 1690 and 1650 marks the presence of Quinone or conjugated ketone compound. This indicates the shift in bandwidth after the synthesis of silver nanoparticles (Karwa et al., 2011). FTIR spectral measurements help identify the potential biomolecules responsible for reducing and capping the bio reduced silver nanoparticles. The peaks recorded at 1376 cm^{-1} indicates the presence of amino groups which are utilized for the encapsulation and stabilization of AgNPs (Preetha et al., 2013).

3.5. XRD analysis

XRD measurements (Fig. 6) of synthesized AgNPs showed peaks at (2θ) ranging from 20 to 80. Three main peaks noted at 2θ were 38.4, 65.1, and 76.8 and their corresponding intensity was at 100, 220, and 311 planes, respectively. The XRD data obtained was matched with inorganic crystal structure database and international center for diffraction data using PDXL-2 software. While comparing the results of XRD spectrum obtained during the present study with the standard, the silver nanoparticles in the prepared sample were having a face-centered cubic crystal structure (FCC) based on one silver atom. The lattice parameter was 0.409 nm. The silver nanoparticles' average crystalline size was estimated using the Debye–Scherer's equation, and it was 18 nm. In addition to the three prominent peaks, weaker peaks of other bioorganic compounds occurring on the surface of the AgNPs were noted. Using Nanosight LM20 (NTA) software the silver nanoparticle synthesized using *G. lucidum* was found in the range10-70 nm with an average size of 45 nm (Karwa et al., 2011). The XRD analysis results indicate that the synthesized nanoparticles are in the size 28 nm. There are several reports that the smaller sized nanoparticles are highly active with antimicrobial potential. The smaller sized nanoparticles penetrate the bacterial cell membrane easily and damage the cellular machinery's respiratory chain. As a result, oxidative stress develops and affects the functioning of DNA and RNA paralyzing the cell division and leads to cell death (Sandhu et al., 2018; Muramatsu et al., 2018; Kamali et al., 2020).

3.6. SEM analysis

The surface morphology and size of the silver nanoparticles were examined using SEM. The SEM images of the synthesized silver nanoparticles in different magnifications is given in Fig. 7(a–e). SEM analysis results indicated that the shape of the individual nanoparticles was predominantly spherical and ploy disperses in nature, as reported (Chowdhury et al., 2014). However, a small aggregation of particles with no well-defined morphology was also seen (Fig. 7a–b). The surface of the particles was smooth

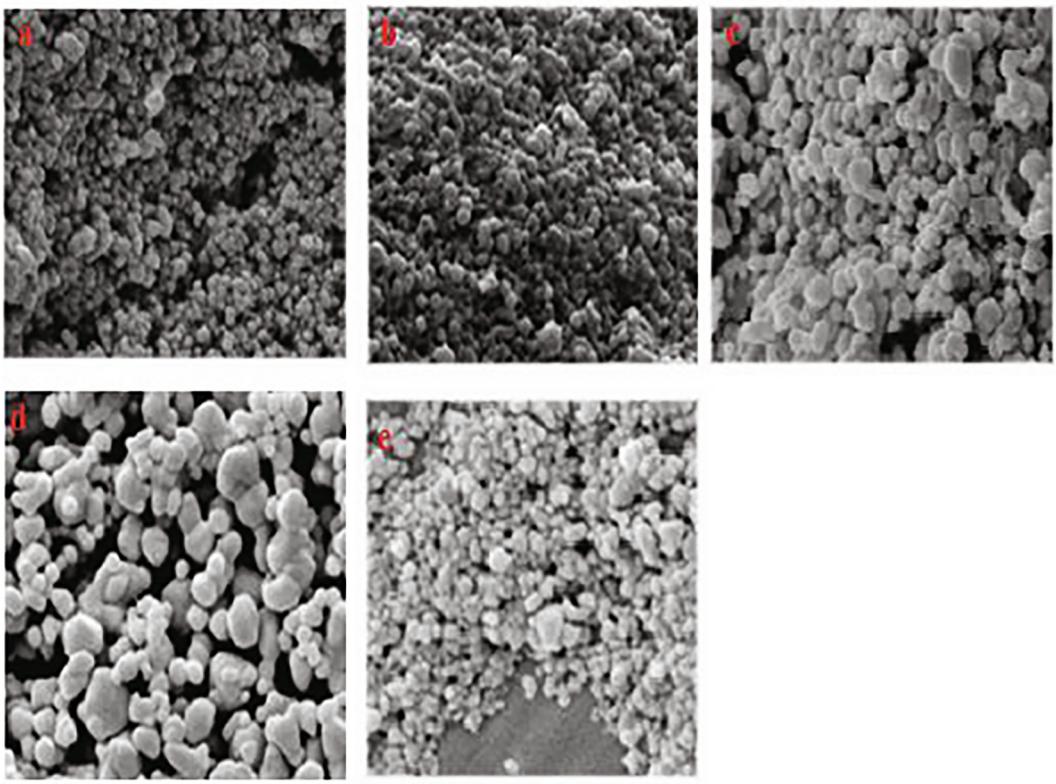

Fig. 7. SEM images of GL-NPs showing their morphology at different resolutions. (a–e): (a & b) SEM of GL-NPs captured at 600× magnification. (c & e) SEM of GL-NPs captured at 16,000× magnification. (d) SEM of GL-NPs captured at 40,000× magnification.

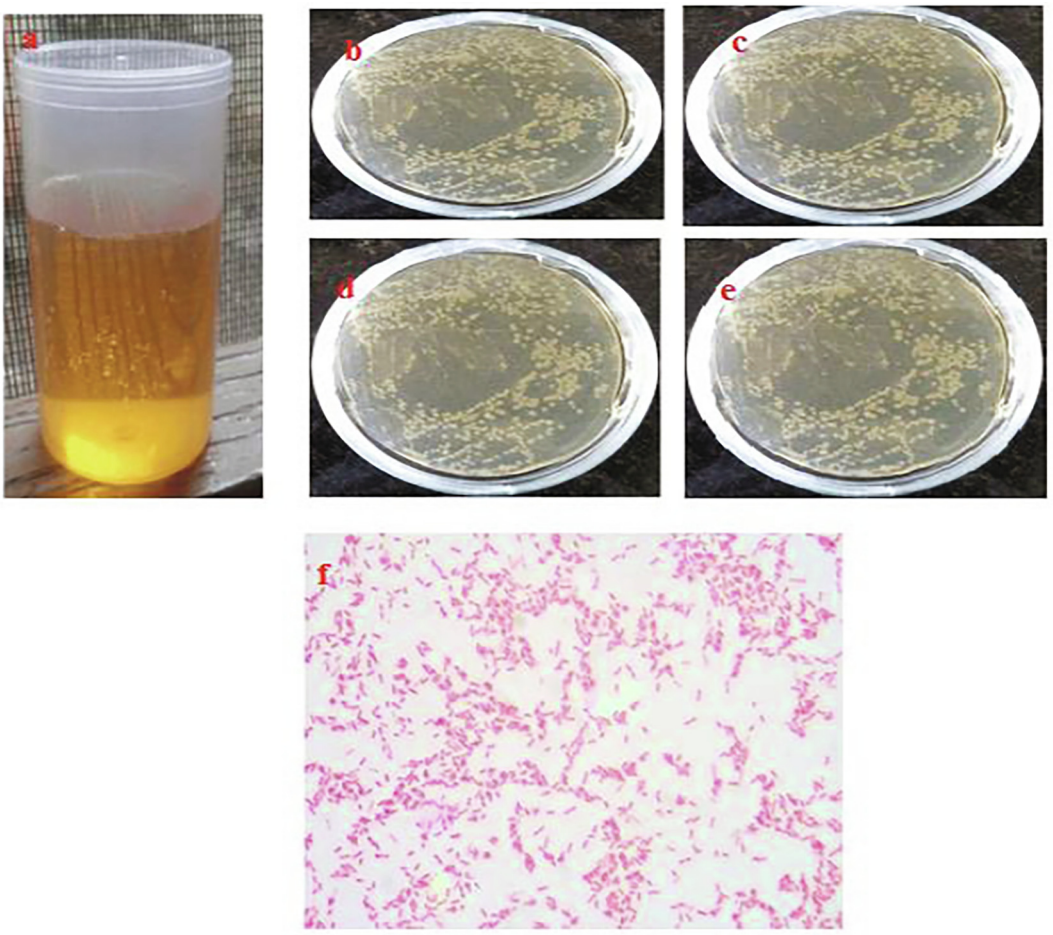

Fig. 8. (a) Collection of urine sample; (b–e) *E. coli* isolated from urine sample of four different patients; (f) Confirmative analyses of *E. coli* by microscopic image of Gram staining.

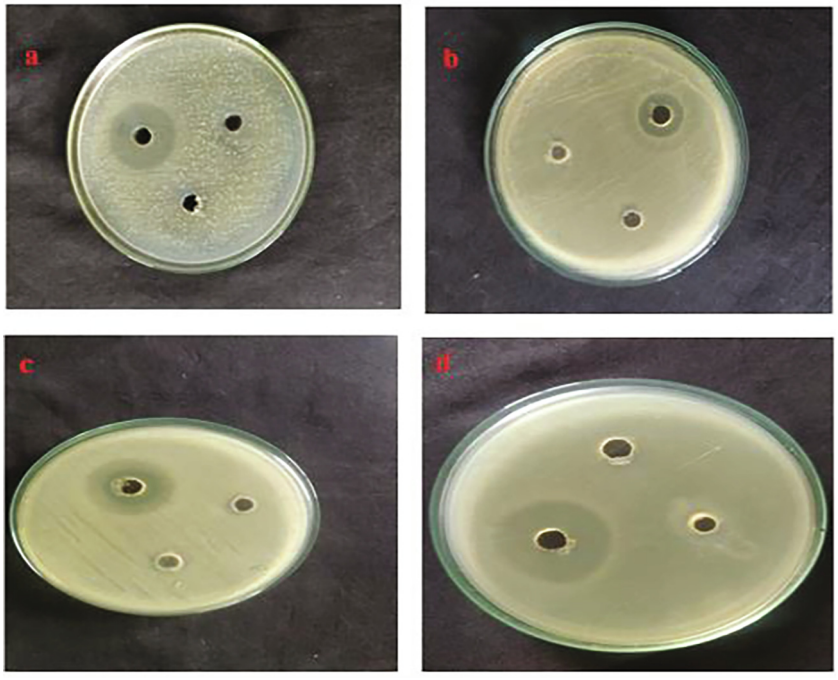

Fig. 9. (a–d) Zone of inhibition in MHA plates with wells filled with 25, 50 and 75 μL of GL-AgNPs: (a) plate inoculated with drug resistant *E. coli* (E1); (b) plate inoculated with *E. coli* (E5); (c) plate inoculated with *E. coli* (E3); (d) plate inoculated with *E. coli* (E4).

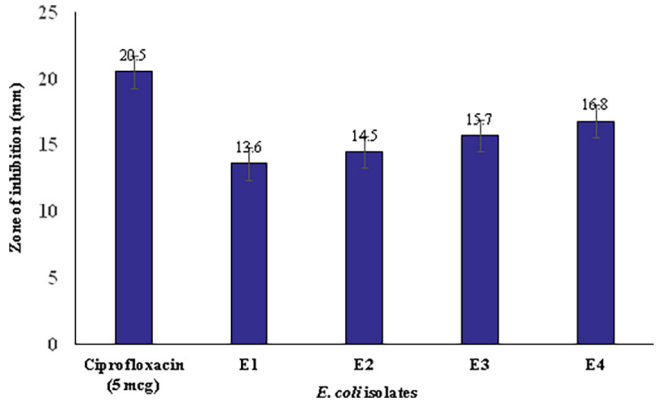

Fig. 10. Antimicrobial activity of GL-AgNPs (effective activity only with concentration of 75 μL) against drug resistant *E. coli* isolates.

(Fig. 7c–e). The particles were in size range between 23 and 58 nm. The spherical shape of AgNPs with an average size of 20–25 nm was reported for biosynthesized silver nanoparticles using the mushroom *G. applanatum* AgNPs (Jogaiaha et al., 2019). The silver nanoparticles synthesized using *G. lucidum* were said to be identically spherical with the size ranging from ~5–30 nm (Ranjith et al., 2017) 10–30 nm by Milan et al. (2017) and ~45 nm by Mohanta Yugal et al. (2017). Against many previous studies, Mohanta et al., (2016) report that the AgNPs synthesized using *G. lucidum* had a largest size range of 133.0 ± 0.361 nm. But in the present study, the GL-AgNPs size range was between 23 and 58 nm, and the reduced size range enhances the antimicrobial potency. The nanoparticles' shape was reported to influence the conjugation with specific drug molecules and target to the cells (Mohanta Yugal et al., 2017). The aggregation of nanoparticles was said to be due to secondary metabolites. However, within the aggregates, the fusion or close contact among them was no noted (Fig. 7. d], and this is indicative of the stabilization of *nanoparticles* due to capping around them as reported (Chowdhury et al., 2014; Pandey et al., 2020).

3.7. Antimicrobial activity

The antimicrobial activity of the *Ganoderma* mediated silver nanoparticles was tested against *E. coli* isolated from urinary tract infection associated catheter indwelled cases. The identification of *E. coli* strain was shows in Fig. 8, such as collection of urine sample (b-e) *E. coli* isolated from urine sample of four different patients (f) Confirmative analyses of *E. coli.* By microscopic image of Gram staining. Three different doses 25, 50 and 75 μL of GL-AgNPs were used -against four *E. coli* isolates using well diffusion method. The maximum zone of inhibitions was observed at the 75 μL concentration of GL-AgNPs. The diameter range of inhibition zone was 13.6–16.8 mm (Figs. 9 and 10). The size of the zone of inhibition varies because of the 4 different isolates of *E. coli*. Milan et al. (2017) reported that the colloidal silver nanoparticles prepared using the extracts of *Ganoderma lucidum* inhibited the growth of *Escherichia coli* (10.1 ± 0.2 mm). When the synthesized AgNPs were mixed with antibiotics like gentamycin and streptomycin, 3.2–3.5 fold increase was reported in the in inhibition activity (Milan et al. 2017). Jogaiaha et al. (2019) found the AgNPs synthesized using the mushroom *Ganoderma applanatum* methanol extracts to show a maximum inhibition of the bacteria *S. aureus* with 18.50 mm inhibition zone and also the inhibition of the fungi *C. capsici* with 75.49% inhibition rate. AgNPs synthesized using *G. lucidum* exhibited an excellent antimicrobial action. Nearly 90% inhibition against four gram-positive strains and the gram-negative E. coli WAS NOTED (Mohanta et al., 2018). The contribution of the bioactive compounds in the mushroom *G. lucidum* in converting the AgNPs with cap and reducing property interfere with the functional mechanism of *E. coli. In this era of growing multidrug resistan*ce in microbes, the silver nanoparticles can be a good alternative as reported. The biologically synthesized NPs using *G. lucidum* extract in the present study report capping agents on the surface of the nanoparticles and that "protein corona", promotes attachment, permeability into *E. coli* cells. As a result, oxidative stress develops in the bacterial pathogen ending in pathogenic killing. The *G. lucidum* inspired AgNPs initiated DNA cleavage activity for 30 and 60 min at 50 and 100 mg/L, a *G. lucidum* extract dose (Aygüna et al., 2020).

3.8. DPPH free radical scavenging activity

The antioxidant capacity of the synthesized AgNPs was tested using DPPH free radical scavenging activity. (Table 2). The percentage scavenging activity of DPPH free radicle expressed as EC50 (Efficient Concentration-μg/ml) showed a progressive increase in the amount of GL-aGnpS dose quercetin concentrations. The percentage scavenging activity was35.73 ± 0.55% at 5 μg/ml dose of AgNPs, and it was 62.18 ± 1.44% at 25 μg/ml dose of AgNPs. The standard antioxidant quercetin, the free radicle scavenging activity, was 50.16 ± 1.20% at 25 μg/ml concentration. The study shows the supremacy of AgNPs in scavenging the free radicals over quercetin. When adding AgNPs in the DPPH solution, a color change was noticed due to the scavenging action of DPPH. This is because of the donation of a hydrogen atom to stable the DPPH molecule. The elemental components in *G. rubidium*'s extract adhering to the formed NPs were reported to exhibit a rich free radical scavenging activity (He et al. 2017). The free radical scavenging ability of biogenic silver nanoparticles is said to be associated with the integration of existed functional groups onto the surface of biogenic AgNPs originated from plant extract (He et al., 2017). From the lower EC50 for AgNPs, the synthesized NPs show a good free radical scavenging activity than the standard antioxidant quercetin as reported (Mishra et al., 2012; Boly et al., 2016).

3.9. Anticancer activity

The cell viability assay is useful to get information on cell death, survival, and metabolic activities due to toxic intrusions (Asha Rani et al., 2009; Chaves et al., 2019). There are many reports that the silver nanoparticles are exhibiting cytotoxicity in a dose-

Table 2
Free radical scavenging activity of GL-AgNPs.

Concentration of GL-AgNPs and quercetin (μg/mL)	Absorbance at 517 nm (GL-AgNPs)	Percent DPPH scavenging	Absorbance at 517 nm (quercetin)	Percent of DPPH scavenging effect
5.0	0.804 ± 0.01	35.73 ± 0.55	0.767 ± 0.03	30.23 ± 0.71
10.0	0.851 ± 0.02	45.94 ± 1.65	0.806 ± 0.01	37.45 ± 0.57
15.0	0.943 ± 0.01	54.05 ± 1.13	0.832 ± 0.02	45.86 ± 1.33
20.0	1.012 ± 0.03	66.77 ± 2.2 6	0.894 ± 0.02	52.53 ± 1.77
25.0	0.984 ± 0.01	62.18 ± 1.44	0.865 ± 0.01	50.16 ± 1.20

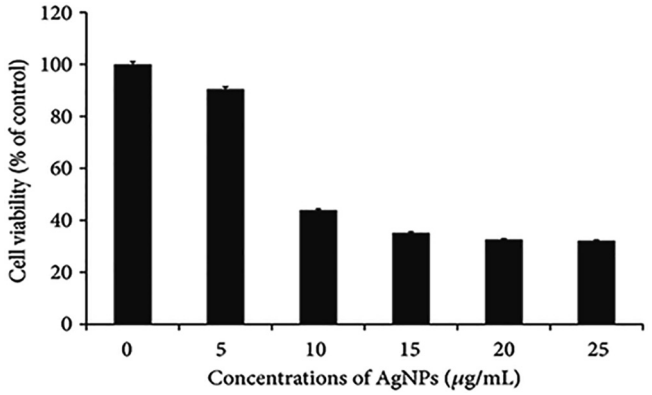

Fig. 11. Cytotoxic effect of different concentrations of GL-AgNPs on MDA-MB-231 cells in the MTT assay.

dependent manner (Devanesan et al., 2020; Alfuraydi et al., 2019; AlSalhi et al., 2016) in human tumor cell lines. In the AgNPs treated cells, decreased metabolic activity was observed, and it varied with the nature of cell types and the size of nanoparticles (Ahmad et al., 2008; Devanesan et al., 2018). In the present study, the chosen breast cancer cell lines were treated with different doses of (5, 10, 15, 25, and 100 μg/mL) GL-AgNPs for 24 h. From the results, it was observed that the GL-AgNPs reduced the cell viability of MDA-MB-231 cells in a dose-dependent manner. At 24 h of treatment, the GL-AgNPs treatment was found to induce cytotoxic effect from 24 h of therapy even at a concentration of 10 μg/mL, and the effect increased with the doses of GL-AgNPs (Fig. 11). The present finding of culture time and concentration-dependent function of GL-AgNPs was reported by other workers (Gurunathan et al., 2013; Korangath et al., 2020).

The half-maximal inhibitory concentration (IC50) is the concentration needed to inhibit the growth of 50% of tumor cells in a culture about the untreated cells. In the present study, GL-AgNPs at a concentration of 9.2 μg/mL decreased fifty percent (IC50) of MDA-MB-231 cells' viability. If the exposure duration and the concentrations are increased, toxicity to the cells also increased. An earlier worker reported a IC50 value of 27 μg/mL in BHK21 (non-cancer) and HT29 (cancer) cells (Gurunathan et al., 2013). Zanette et al. (2011) also reported a IC50 value 6.8 ± 1. The μM of GL-AgNPs on cancer cell lines in MTT assay and 12 ± 1.2 μM in SRB assay. The IC50 results also have a relationship with the size, shape, media condition, cell type doses of NPs, and treatment duration (Park et al., 2010; Nishanth et al., 2011).

4. Conclusion

The present study suggested that the silver nanoparticles synthesized using ethanol extract of a medicinal mushroom *G. lucidum* exhibited a multifocal biomedical potential. The presence of l,4-Dioxane-2,3-diol, Ethyl acetoacetate ethylene acetal, and Pyridin-3-ol in the mushroom engineered the silver nanoparticles with antimicrobial, antioxidant and anti-tumor activities. The drug-resistant *E. coli* was highly sensitive to the synthesized GL-AgNPs. The findings of this study provide valuable application information for a lead nanoparticle that can be eco-friendly and cost-effective to fight drug-resistant microbes and cancer.

Declaration of Competing Interest

The authors declare that they have no known competing financial interests or personal relationships that could have appeared to influence the work reported in this paper.

Acknowledgement

The authors extend their appreciation to the Researchers Supporting Project number (RSP-2020/228), King Saud University, Riyadh, Saudi Arabia.

References

Ahmad, P., Sarwat, M., Sharma, S., 2008. Reactive oxygen species, antioxidants and signaling in plants. J. Plant Biol. 51, 167–173.
Alfuraydi, A.A., Devanesan, S., Al-Ansari, M., AlSalhi, M.S., Ranjitsingh, A.J., 2019. Eco-friendly green synthesis of silver nanoparticles from the sesame oil cake and its potential anticancer and antimicrobial activities. J. Photochem. Photobiol. B 192, 83–89.
Aranzazu, G., Violeta, A., Alegria, M., Jose, M.S., 2020. Review: Use of *Ganoderma lucidum* (Ganodermataceae, Basidiomycota) as Radioprotector. Nutrients 12, 1143.
AlSalhi, M.S., Devanesan, S., Alfuraydi, A.A., Vishnubalaji, R., Munusamy, M.A., Murugan, K., Nicoletti, M., Benelli, G., 2016. Green synthesis of silver nanoparticles using *Pimpinella anisum* seeds: antimicrobial activity and cytotoxicity on human neonatal skin stromal cells and colon cancer cells. Int. J. Nanomed. 11, 4439–4449.
Asha Rani, P.V., Low Kah Mun, G., Hande, M.P., Valiyaveettil, S., 2009. Cytotoxicity and genotoxicity of silver nanoparticles in human cells. ACS Nano 3, 279–290.
Aygüna, A., Özdemir, S., Gülcan, M., Cellata, K., Şen, F., 2020. Synthesis and characterization of Reishi mushroom-mediated green synthesis of silver nanoparticles for the biochemical applications. J. Pharmaceut. Biomed. 178, 112970.
Bergey, D.H., Holt, J.G., 2000. Bergey's Manual of Determinative Bacteriology. Lippincott Williams & Wilkins, Philadelphia, USA.
Bhani, D., Bachhiwal, R., Sharma, R., Maheshwari, R.K., 2017. Microbial profile and antimicrobial susceptibility pattern of uropathogens isolated from catheter associated urinary tract infection (CAUTI). Int. J. Curr. Microbiol. Appl. Sci. 6, 2446–2453.
Bharadwaj, S., Lee, K.E., Dwivedi, V.D., et al., 2019. Discovery of *Ganoderma lucidum* triterpenoids as potential inhibitors against Dengue virus NS2B-NS3 protease. Sci. Rep. 9, 19059.
Boly, R., Lamkami, T., Lompo, M., Dubois, J., Guissou, P., 2016. DPPH Free Radical Scavenging Activity of Two Extracts from *Agelanthus dodoneifolius* (Loranthaceae) Leaves. Int. J. Toxicol. Pharmacol. Res. 8, 29–34.
Chaves, N.L., Amorim, D.A., Lopes, C.A.P., et al., 2019. Comparison of the effect of rhodium citrate-associated iron oxide nanoparticles on metastatic and non-metastatic breast cancer cells. Cancer Nanotechnol. 10, 7.
Chowdhury, S., Basu, A., Kundu, S., 2014. Green synthesis of protein capped silver nanoparticles from phytopathogenic fungus *Macrophomina phaseolina* (Tassi) Goid with antimicrobial properties against multidrug-resistant bacteria. Nanoscale Res. Lett. 9, 365.
Cilerdzic, J.L., Sofrenic, I.V., TeSevic, V.V., et al., 2018. Neuroprotective potential and chemical profile of alternatively Cultivated Ganoderma lucidum Basidiocarps. Chem. Biodivers. 15, 1800036.
Cor, D., Knez, Z., Hrncic, M., 2018. Antitumour, antimicrobial, antioxidant and antiacetyl cholinesterase effect of *Ganoderma lucidum* terpenoids and polysaccharides: A review. Molecules 23, E649.
Devanesan, S., AlSalhi, M.S., Balaji, R.V., Ranjitsingh, A.J.A., Ahamed, A., Alfuraydi, A. A., AlQahtani, F.Y., Aleanizy, F.S., Othman, A.H., 2018. Antimicrobial and cytotoxicity effects of synthesized silver nanoparticles from *Punica granatum* Peel Extract. Nanoscale Res. Lett. 13, 315.
Devanesan, S., Ponmurugan, K., AlSalhi, M.S., Al-Dhabi, N.A., 2020. Cytotoxic and antimicrobial efficacy of silver nanoparticles synthesized using a traditional phytoproduct, asafoetida gum. Int. J. Nanomed. 15, 4351–4362.
Gurunathan, S., Han, J.W., Vasuki, E., Muniyandi, J., Jin-Hoi, K., 2013. Cytotoxicity of biologically synthesized silver nanoparticles in MDA-MB-231 human breast cancer cells. Biomed Res. Int. Article ID 535796.
Harding, J.L., Reynolds, M.M., 2014. Combating medical device fouling. Trends Biotechnol. 32, 140–146.
Muramatsu, K., Fujino, Y., Kubo, T., Otani, M., Fushimi, K., Matsuda, S., 2018. Efficacy of antimicrobial catheters for prevention of catheter-associated urinary tract infection in acute cerebral infarction. J. Epidemiol. 28, 54–58.
He, Y., Wei, F., Ma, Z., Zhang, H., Yang, Q., Yao, B., et al., 2017. Green synthesis of silver nanoparticles using seed extract of Alpinia katsumadai, and their antioxidant, cytotoxicity, and antibacterial activities. RSC Adv. 7, 39842–39851.
Hrvatin, V., 2017. Combating antibiotic resistance: New drugs or alternative therapies? Can. Med. Assoc. J. 189, E1199.
Inamuddin, K.S., 2020. One-pot biosynthesis of silver nanoparticle using Colocasia esculenta extract: Colorimetric detection of melamine in biological samples. J. Photochem. Photobiol. 391.
Inga, K., Maria, M., Miroslawa, S., Anna, G., 2007. Effect of storage on the content of polyphenols, vitamin C and the antioxidant activity of orange juices. J. Food Compost. Anal. 20, 313–332.
Jogaiaha, S., Mahantesh, K., Mostafa, A., Nagabhushan, H., Lam-Son, P.T., 2019. *Ganoderma applanatum*-mediated green synthesis of silver nanoparticles: Structural characterization, and *in vitro* and *in vivo* biomedical and agrochemical properties. Arab. J. Chem. 12, 1108–11011.

Kamali, E., Jamali, A., Ardebili, A., Freshteh Ezadi, F., Mohebb, A., 2020. Evaluation of antimicrobial resistance, biofilm forming potential, and the presence of biofilm-related genes among clinical isolates of *Pseudomonas aeruginosa*. BMC Res. Notes 13, 27.

Kannan, M., Padmanaban, M., Uthayakumar, V., Jayakumar, R., 2014. Mycosynthesis, Characterization and Antibacterial activity of Silver Nanoparticles (Ag-NPs) from fungus *Ganoderma lucidum*. Malaya. J. Biosci. 1, 134–142.

Karwa, A., Swapnil, G., Mahendra Rai, S., 2011. Mycosynthesis of silver nanoparticles using lingzhi or reishi medicinal mushroom, *Ganoderma lucidum* (W. Curt.:Fr.) P. Karst. and their role as antimicrobials and antibiotic activity enhancers. Int. J. Med. Mushrooms. 13, 483–491.

Kaul, G., Shukla, M., Dasgupta, A., Chopra, S., 2019. Alternative therapies to antibiotics to combat drug-resistant bacterial pathogens. In: Ahmad, I., Ahmad, S., Rumbaugh, K. (Eds.), Antibacterial Drug Discovery to Combat MDR. Springer, Singapore.

Kim, B., Pai, H., Choi, W.S., Kim, Y., Kweon, K.T., Kim, H.A., Ryu, S.Y., Wie, S.H., Kim, J., 2017. Current status of indwelling urinary catheter utilization and catheter-associated urinary tract infection throughout hospital wards in Korea: A multicenter prospective observational study. PloS One 12, e0185369.

Korangath, P., Barnett, J.D., Sharma, A., et al., 2020. Nanoparticle interactions with immune cells dominate tumor retention and induce T cell–mediated tumor suppression in models of breast cancer. Sci. Adv. 6. eaay1601.

Liu, Z., Xing, J., Zheng, S., et al., 2016. Ganoderma lucidum polysaccharides encapsulated in liposome as an adjuvant to promote Th1-bias immune response. Carbohydr. Polym. 142, 141–148.

Milan, P., Rabin, P., Sudip, K.C., Suvash, C.A., Rajaram, P., 2017. Biosynthesis of silver nanoparticles using *Ganoderma lucidum* and assessment of antioxidant and antibacterial activity. Int. J. Appl. Sci. Biotechnol. 5, 523–531.

Mishra, K., Ojha, H., Chaudhury, N.K., 2012. Estimation of antiradical properties of antioxidants using DPPH assay: A critical review and results. Food Chem. 130, 1036–1043.

Moghaddam, A., Namvar, F., Moniri, M., Tahir, P., Azizi, S., Mohamad, R., 2015. Nanoparticles biosynthesized by fungi and yeast: a review of their preparation, properties, and medical applications. Molecules 20, 16540–16565.

Mohanta Yugal, K., Panda Sujogya, K., Bastia Akshaya, K., Mohanta Tapan, K., 2017. Biosynthesis of silver nanoparticles from *Protium serratum* and investigation of their potential impacts on food safety and control. Front. Microbiol. 8, 626.

Mohanta, Y.K., Nayak, D., Biswas, K., et al., 2018. Silver nanoparticles synthesized using wild mushroom show potential antimicrobial activities against food borne pathogens. Molecules 23, 655.

Mohanta, Y.K., Singdevsachan, S.K., Parida, U.K., Panda, S.K., Mohanta, T.K., Bae, H., 2016. Green synthesis and antimicrobial activity of silver nanoparticles using wild medicinal mushroom *Ganoderma applanatum* (Pers.) Pat. from Similipal Biosphere Reserve, Odisha,India. IET Nanobiotechnol. 10, 184–189.

Nanhui, Y., Yongpan, H., Yu, J., Lianhong, Z., Xiehong, L., Sulai, L., Fang, C., Jun, L., Yimin, Z., 2020. Ganoderma lucidum Triterpenoids (GLTs) reduce neuronal apoptosis via inhibition of ROCK signal pathway in APP/PS1 transgenic Alzheimer's disease mice. Oxid. Med. Cell. Longev. 2020. ID 9894037.

Nice, 2009. Guidelines Urinary tract infection (catheter-associated): antimicrobial prescribing Publishing, Green J-BD, Fulghum T, Nordhaus MA. Immobilized antimicrobial agents: A critical perspective. Chem. Rev. 109, 5437–5527.

Nishanth, R.P., Jyotsna, R.G., Schlager, J.J., Hussain, S.M., Reddanna, P., 2011. Inflammatory responses of RAW 264.7 macrophages upon exposure to nanoparticles: role of ROS-NFκB signaling pathway. Nanotoxicology 5, 502–516.

Olivares, E., Stéphanie Badel-Berchoux, S., Provot, C., Prévost, G., Bernardi, T., Jehl, F., 2020. Clinical impact of antibiotics for the treatment of *Pseudomonas aeruginosa* biofilm infections. Front. Microbiol. 10, 2894.

Pandey, S., De Klerk, C., Kim, J., Kang, M., Fosso-Kankeu, E., 2020. Eco friendly approach for synthesis, characterization and biological activities of milk protein stabilized silver nanoparticles. Polymers 12, 1418.

Park, E.-J., Yi, J., Kim, Y., Choi, K., Park, K., 2010. Silver nanoparticles induce cytotoxicity by a Trojan-horse type mechanism. Toxicol. In Vitro 24, 872–878.

Preetha, D., Kumari, P., Aarti, C., Arun, R., 2013. Synthesis and characterization of silver nanoparticles using cannonball leaves and their cytotoxic activity against MCF-7 cell line. Nanocomposites 2013, 598328.

Ranjith, D., Santhosh Kumar, S., Senthilkumar, P., Surendran, L., Sudhagar, B., 2017. *Ganoderma lucidum*- oriental mushroom mediated synthesis of gold nanoparticles conjugated with doxorubicin and evaluation of its anticancer potential on human breast cancer MCF-7/DOX cells. Int. J. Pharm. Pharm. Sci. 9, 267–274.

Roy, A., Onur, B., Sudip, S., Amit Kumar, M., Deniz, M., 2019. Green synthesis of silver nanoparticles: biomolecule-nanoparticle organizations targeting antimicrobial activity. RSC Adv. 9, 2673.

Sabih, A., Leslie, S.W., 2020. Complicated Urinary Tract Infections. StatPearls [Internet]. Stat Pearls Publishing, Treasure Island (FL).

Sánchez-López, E., Gomes, D., Esteruelas, G., Bonilla, L., Lopez-Machado, A.L., Galindo, R., Cano, A., Espina, M., Ettcheto, M., Camins, A., Silva, A.M., Durazzo, A., Santini, A., Garcia, M.L., Souto, E.B., 2020. Metal-based nanoparticles as antimicrobial agents: An overview. Nanomaterials 10, 292.

Sandhu, R., Sayal, P., Jakkhar, R., Sharma, G., 2018. Catheterization-associated urinary tract infections: Epidemiology and incidence from tertiary care hospital in Haryana. J. Health Res. Rev. 5, 135–141.

Scott, D., Toney, M., Muzikár, M., 2008. Harnessing the mechanism of glutathione reductase for synthesis of active site bound metallic nanoparticles and electrical connection to electrodes. J. Am. Chem. Soc. 130, 865–874.

Zaheer, Z., Rafiuddin, 2012. Silver nanoparticles to self-assembled films: green synthesis and characterization. Colloid. Surf. B 90, 48–52.

Zanette, C., Pelin, M., Crosera, M., Adami, M., Bovenzi, G., Larese, F., Florio, C., 2011. Silver nanoparticles exert a long-lasting antiproliferative effect on human keratinocyte HaCaT cell line. Toxicol. In Vitro 25, 1053–1060.

Zhang, X.F., Liu, Z.G., Shen, W., Gurunathan, S., 2016. Silver nanoparticles: synthesis, characterization, properties, applications, and therapeutic approaches. Int. J. Mol. Sci. 17, E1534.

Zhang, W., Tao, J., Yang, X., Yang, Z., Zhang, L., Liu, H., Wu, K., Wu, J., 2014. Antiviral effects of two Ganoderma lucidum triterpenoids against enterovirus 71 infection. Biochem. Biophys. Res. Commun. 449, 307–312.